Efficient and robust waveform-inversion workflow: Tomographic FWI followed by FWI

Biondo Biondi and Ali Almomin

ABSTRACT

In many important practical cases when FWI convergence is uncertain because of the lack of low-frequency data and/or long offsets, we would like to employ waveform-inversion methods, such as tomographic FWI (TFWI), that offer more robust convergence. However, the additional computational cost can be a serious deterrent form applying TFWI to the full bandwidth of the data. As an alternative, we propose the following cost-effective TFWI+FWI workflow: 1) TFWI applied to the low frequencies in the data, 2) FWI applied to the high frequencies starting from the model estimated by TFWI. We tested TFWI+FWI on two synthetic datasets computed from the Marmousi 2 model by comparing the results obtained by full-bandwidth TFWI with models obtained by the proposed workflow when TFWI was applied to data low-passed to a maximum of 10 Hz. The new workflow converged to very accurate models even when conventional FWI with frequency continuation failed. Further cost-saving can be achieved by switching from TFWI to FWI before TFWI reaches full convergence. Depending on the number of TFWI iterations, the quality of the final model is negatively affected but it can be still satisfactory.

INTRODUCTION

Full waveform inversion (FWI) (Bamberger et al., 1982; Tarantola, 1984) has the potential of overcoming the limitations imposed by the conventional sequential seismic-imaging workflow of velocity analysis followed by migration. However, FWI convergence is notoriously dependent on the accuracy of the starting velocity model and/or the availability of low-frequency data. In many cases, when these conditions are not fulfilled, the tomographic component of the inversion is subject to cycle-skipping and convergence is uncertain.

To overcome FWI convergence problems, FWI and wave-equation migration velocity analysis (WEMVA) can be successfully integrated and simultaneously performed. Tomographic FWI (TFWI) is a robust and self-consistent approach to integrate the two phases by extending the velocity model along either the subsurface-offset or the time-lag axes and adding a term to the FWI objective function that rewards image focusing (Symes, 2008; Sun and Symes, 2012; Biondi and Almomin, 2012, 2013, 2014).

However, TFWI adds computational cost to the already computational-intensive FWI process.

The computational cost added by time-lags TFWI (Biondi and Almomin, 2014) grows linearly with the frequency in the data. This frequency dependency compounded with FWI exponential growth with frequencies, may prevent TFWI large-scale applications to the whole data bandwidth until further improvements in computational systems become available. This observation suggests the development and the testing of a practical waveform-inversion workflow that employs TFWI only on the lower frequency in the data, and then switches to conventional FWI for the higher frequencies. By applying TFWI instead of FWI to the lower frequency we are more likely avoid falling in local minima related to the long wavelengths of the velocity model. After the model long-wavelength components are estimated by TFWI with sufficient accuracy to explain the kinematics in the low-frequency data, the use of FWI with frequency continuation (i.e. by slowly increasing the bandwidth of the data starting from the low end of the range) for the higher frequencies should be safe and improve the resolution of the final model.

The main theoretical limitation of the proposed solution is that the resolution of the tomographic component of TFWI is directly proportional the data frequency, and thus it is suboptimal when only the low frequencies are used. By limiting the application of TFWI to the low frequencies we leave the inversion of the tomographic component present in the data high frequencies to the less robust FWI. We implicitly assume that at the moment of the switch from TFWI to FWI the long-wavelength in the model are not only sufficiently accurate to explain the kinematics at low frequencies, but also sufficiently accurate to prevent FWI to fall in a local minimum. The results of the synthetic-data tests shown in this abstract confirm the validity of the suggested workflow, and warrant further testing with field data.

TFWI+FWI WORKFLOW

Biondi and Almomin (2014) introduce TFWI by extending the velocity model along the time-lag axis τ. To reduce the additional computational burden, the time-lag extension is introduced only in the evaluation of the discretized linearized operator $\widetilde{\mathbf{L}}$ as follows:

$$\left[\tilde{\mathbf{S}}_o^2(\tau=0)\,\mathbf{D_2} - \nabla^2\right]\delta\mathbf{w} = \delta\tilde{\mathbf{S}}^2(\tau) \overset{\tau}{*} \mathbf{D_2 w_o}, \tag{1}$$

where $\mathbf{w_o}$ and $\delta\mathbf{w}$ are the background and perturbed wavefields, respectively; $\tilde{\mathbf{S}}_o$ and $\delta\tilde{\mathbf{S}}$ are diagonal matrices that are formed from the corresponding elements of the discretized background and perturbed extended-slowness models, respectively; $\mathbf{D_2}$ is a discretized second-derivative operator, ∇^2 is a finite-difference approximation of the Laplacian operator, and $\overset{\tau}{*}$ denotes convolution in τ. The full non linear extended modeling operator $\tilde{\mathcal{L}}$ is then defined as follows

$$\tilde{\mathcal{L}}(\tilde{\mathbf{s}}) = \mathcal{L}(\tilde{\mathbf{s}}_o(\tau=0)) + \widetilde{\mathbf{L}}(\tilde{\mathbf{s}}_o(\tau=0))\,\delta\tilde{\mathbf{s}}^2, \tag{2}$$

where $\mathcal{L}$ is the conventional wave-equation operator function only of the non-extended slowness (i.e. $\tilde{\mathbf{s}}_o\,(\tau=0)$, and $\delta\tilde{\mathbf{s}}$ is a vector formed from the elements of the discretized perturbed extended-slowness models. The TFWI objective function is defined as follows:

$$J_{\text{TFWI}}\left(\tilde{\mathbf{s}}\right) = \frac{1}{2}\left\|\tilde{\mathcal{L}}\left(\tilde{\mathbf{s}}\right) - \mathbf{d}\right\|_2^2 + \epsilon\left\||\tau|\,\tilde{\mathbf{s}}^2\right\|_2^2. \tag{3}$$

The first term in this objective function is a FWI-like data-fitting term, with the important difference that because of the slowness-model extension, this term is not sufficient to constraint the solution. The second term in the equation 3 rewards focusing of the model around zero time lag. It introduces a tomographic component that constraints the optimization problem and forces the convergence towards solutions that fit the data and corresponds to well-focused models.

The objective function in equation 3 is minimized using a nested optimization algorithm (Almomin and Biondi, 2014). In the outer iterations the nonlinear modeling operator (equation 2) is evaluated to update the data residuals, whereas in the inner iterations only the linearized operators are evaluated. The computational cost of these iterations is dominated by wave propagation and thus grows with the 4th power of the temporal frequencies. TFWI introduces an additional cost related to the performance of the convolutions along the time-lag axis in equation 1 (or correlations when evaluating the adjoint operator). The computational cost of these convolutions (correlations) is directly proportional to the number of samples used to represented the discretized time-lags axis. The time duration of the time-lag axis necessary to ensure convergence depends on the errors in the initial slowness model and is thus independent from the data frequencies. In contrast, the sampling rate is inversely dependent on the data frequencies, and thus the cost of the convolutions (correlations) grows linearly with the data frequencies.

To reduce the computational cost of a waveform inversion, and still benefiting from the convergence properties of TFWI, we propose a workflow that starts with TFWI applied only to the low frequencies in the data. Once we are confident that the estimated long-wavelength components of the model are sufficiently accurate, we switch to a conventional FWI algorithm to invert the higher frequencies. To minimize the chances of FWI falling into a local minimum when inverting the higher frequencies, we employ the the well-established frequency-continuation approach (Bunks et al., 1995); that is, we slowly increase the bandwidth of the data starting from the low end of the frequency range.

MARMOUSI RESULTS

We tested the accuracy and efficiency of the workflow described in the previous section using two synthetic datasets, both modeled using the Marmousi 2 velocity model (Martin et al., 2002). Figure 1 shows the velocity model used for modeling. The water layer is thicker than in the original Marmousi; this thicker layer reduces the amount of refracted energy being recorded in the data. Therefore, these datasets tests

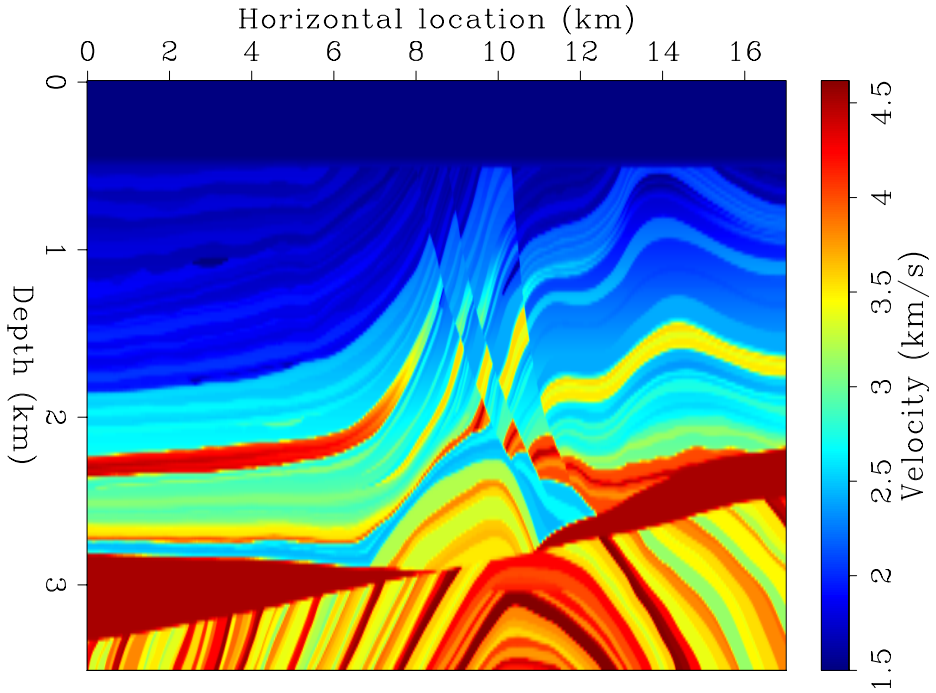

Figure 1: The velocity of the Marmousi 2 model. [**ER**]

the capabilities of the proposed workflow to converge in presence of almost exclusively reflected events.

The two datasets are only different with respect to their low-end frequency limit. The first one was modeled using a bandpassed wavelet with a frequency range between 5 Hz to 25 Hz, whereas the frequency range of the second dataset was between 3 Hz to 25 Hz. The acquisition geometry comprises 851 fixed receivers with a spacing of 20 m and 171 sources with a spacing of 100 m. The data were modeled using a constant-density finite-differences solution of the acoustic wave equation. For all our inversion results, the initial model was a 1D function that started with the water layer and linearly increases with a gradient of .83333 1/s below the water bottom. To demonstrate the convergence improvements achieved by the proposed TFWI+FWI workflow with respect to conventional FWI, we compare the result obtained by three workflows: 1) TFWI for all the frequencies present in the data, 2) FWI with frequency continuation starting from the lowest frequencies present in the data (3 or 5 Hz) and ending at 25 Hz, and 3) TFWI for the lowest frequencies up to 10 Hz, followed by FWI with frequency continuation from 10 Hz to 25 Hz. For workflow 1) we run TFWI for 35 outer iterations, as outlined above and described in more details by Almomin and Biondi (2014). For workflow 3) we run TFWI for 20 outer iterations with the 5-25 Hz data and for 30 iterations with the 3-25 Hz data. As expected, the TFWI results are the best, but also the most expensive. They represent the benchmark with respect to which we measure the results achieved by the two other approaches.

Figure 2 shows the results obtained from the application of the three work-

flows described above to the 5-25 Hz dataset: TFWI (panel a), FWI (panel b), and TFWI+FWI (panel d). It also shows the intermediate model produced by the application of TFWI (panel c) in the TFWI+FWI workflow and used as starting model for the FWI step. Because of the lack of low frequencies in the data, the FWI results show poor focusing and gross mispositioning of most of the subsurface features. They clearly demonstrate the failure of the conventional workflow employing FWI with frequency continuation to estimate the long-wavelength components of the velocity model, and consequently to focus the reflections from the velocity discontinuities. In contrast, the proposed TFWI+FWI workflow (panel d) achieves almost as an accurate result as the more expensive TFWI workflow (panel a). Most of the differences between these two results are located at the edges, where even TFWI fails to recover the model because of lack of "illumination" by the data geometry. These high-quality results are achieved because the long-wavelengths in the model produced by TFWI applied to the data low frequencies ($\leq$10 Hz) (panel c) explains accurately the reflections kinematics and enable the ensuing FWI to converge.

Figure 3 shows the results obtained from the three workflows described above applied to the 3-25 Hz dataset: TFWI (panel a), FWI (panel b), and TFWI+FWI (panel d). Because of the additional low frequencies present in the data, the FWI results show improvements with respect to the previous case (Figure 2b), mostly in the shallow part of the model. However, in the deeper part of the section, in particular in the reservoir area, the reflections are still poorly focused and mispositioned. As for the example above, the proposed TFWI+FWI workflow (panel d) achieves almost as an accurate result as the more expensive TFWI workflow (panel a). In contrast with the previous example, the differences at the edges of the model are minimal, with both methods succeeding to well recover the original model. The improvements in the final results (panel d) are easily understood when comparing the intermediate models produced by the application of TFWI in the TFWI+FWI workflow; that is, when comparing Figure 2c with Figure 3c.

The results shown in the previous figures demonstrate the efficacy of the proposed TFWI+FWI workflow. We reckon that the number of TFWI iterations used for the previous examples (20 outer iterations for the 5-25 Hz dataset and 30 for the 3-25 Hz dataset) extracted from the data the most of the long-wavelength information present up to 10Hz, and enabled FWI to converge when inverting the higher frequencies data. In practice, to further reduce the computational cost, we would like to use even less TFWI iterations. The results shown in Figure 4 illustrates, for the 5-25 Hz dataset, the consequences of stopping TFWI before it converged. Figure 4a shows the model produced by TFWI after 5 outer iterations and Figure 4c shows the model produced by TFWI after 10 outer iterations. Figure 4b shows the results of FWI with frequency continuation when starting from the model shown in Figure 4a. This model is clearly unsatisfactory, in particular on the left side of the section. Figure 4d shows the results of FWI with frequency continuation when starting from the model shown in Figure 4c. This model is much improved with respect to the previous one, although is noticeable worse than the one obtained after running TFWI to full convergence before switching to FWI (Figure 2d). As expected, the quality of the final FWI results are strongly

dependent on the accuracy of the long-wavelength estimates obtained by applying TFWI on the lower-frequencies data.

CONCLUSIONS

We introduced a new waveform-inversion workflow that takes advantage of the strong convergence properties of TFWI but reduces the computational cost by applying the expensive TFWI process only to the low frequencies in the data. A conventional FWI with frequency continuation can then be applied to the higher frequencies starting from the velocity model estimated by the low-frequency TFWI. By performing extensive testing on two synthetic datasets modeled from the Marmousi 2 model, we demonstrate that the new TFWI+FWI workflow is capable of reconstructing the Marmousi 2 model in the absence of the low frequencies necessary for FWI to converge. We also show how the final results degrade as the number of TFWI iterations are reduced; that is, as computational cost decreases. The results of the synthetic-data tests shown in this abstract confirm the validity of the suggested workflow, and warrant further testing with field data.

ACKNOWLEDGMENTS

We would like to acknowledge Frank Agnar Maaø with Statoil for first suggesting the idea of the workflow we presented, the affiliate companies of the Stanford Exploration Project for financial support, and Saudi Aramco for supporting the second author's graduate studies at Stanford.

REFERENCES

Almomin, A. and B. Biondi, 2014, Preconditioned tomographic full waveform inversion by wavelength continuation: SEG Expanded Abstracts, **33**, *submitted for publication*.

Bamberger, A., G. Chavent, C. Hemon, and P. Lailly, 1982, Inversion of normal incidence seismograms: Geophysics, **47**, 757–770.

Biondi, B. and A. Almomin, 2012, Tomographic full waveform inversion (TFWI) by combining full waveform inversion with wave-equation migration velocity anaylisis: SEG Expanded Abstracts, **31**, 275–279.

———, 2013, Tomographic full waveform inversion (tfwi) by extending the velocity model along the time-lag axis: SEG Expanded Abstracts, **32**, 1031–1036.

———, 2014, Simultaneous inversion of full data bandwidth by tomographic full waveform inversion: Geophysics, **79**, *in press*.

Bunks, C., F. Saleck, S. Zaleski, and G. Chavent, 1995, Multiscale seismic waveform inversion: Geophysics, **60**, 1457–1473.

Martin, G., K. Marfurt, and S. Larsen, 2002, Marmousi–2: An updated model for the investigation of avo in structurally complex areas: SEG Technical Program Expanded Abstracts, **21**, 1979–1982.

Sun, D. and W. W. Symes, 2012, Waveform inversion via nonlinear differential semblance optimization: SEG Expanded Abstracts, **31**, 1190–1194.

Symes, W. W., 2008, Migration velocity analysis and waveform inversion: Geophysical Prospecting, **56**, 765–790.

Tarantola, A., 1984, Inversion of seismic reflection data in the acoustic approximation: Geophysics, **49**, 1259–1266.

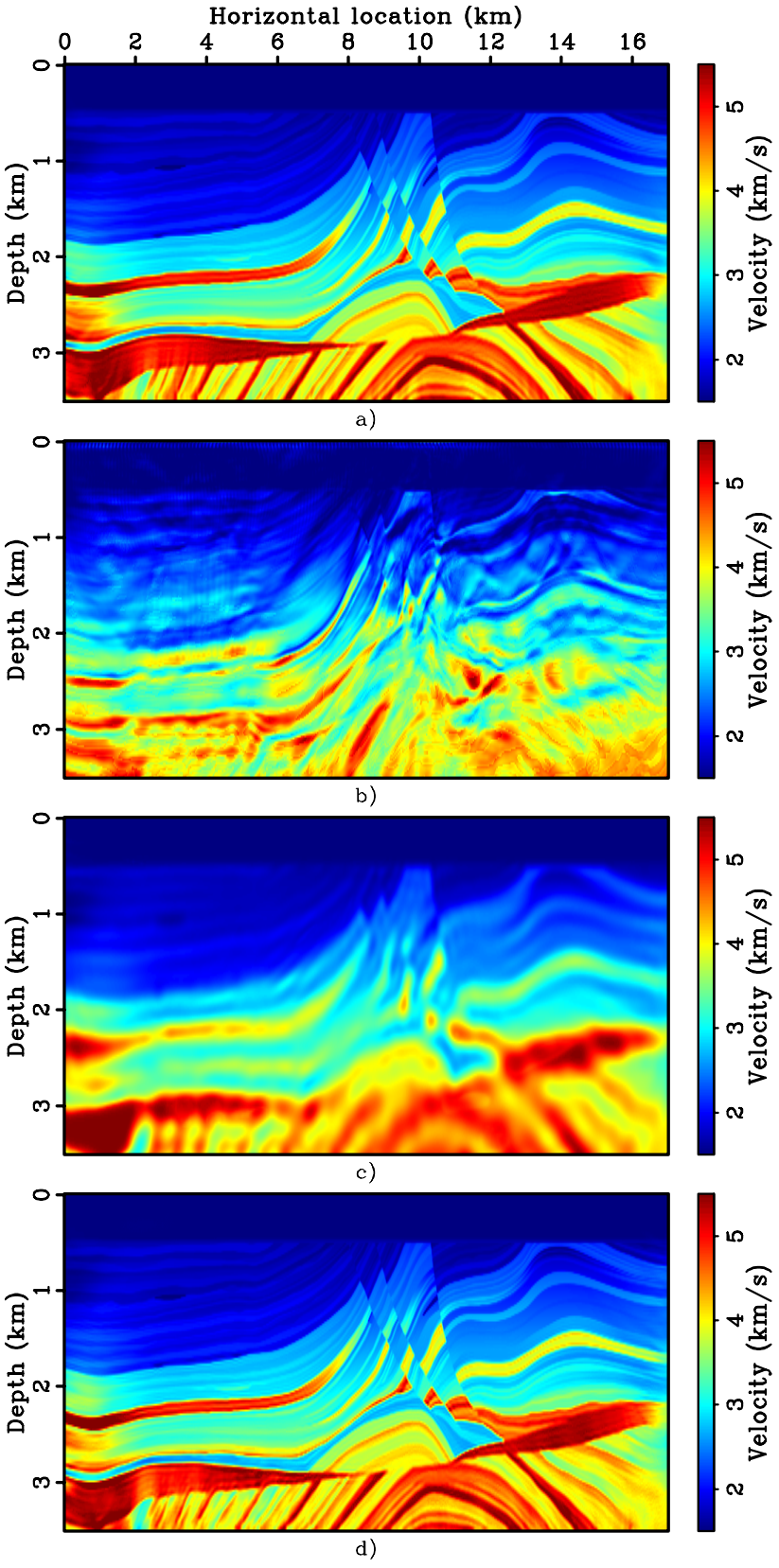

Figure 2: Velocity models estimated from the 5-25 Hz dataset by applying: a) TFWI for the whole bandwidth, b) FWI with frequency continuation starting from 5 Hz data, c) TFWI up to 10 Hz, and d) FWI with frequency continuation starting from 10 Hz data and the model shown in c). [**CR**]

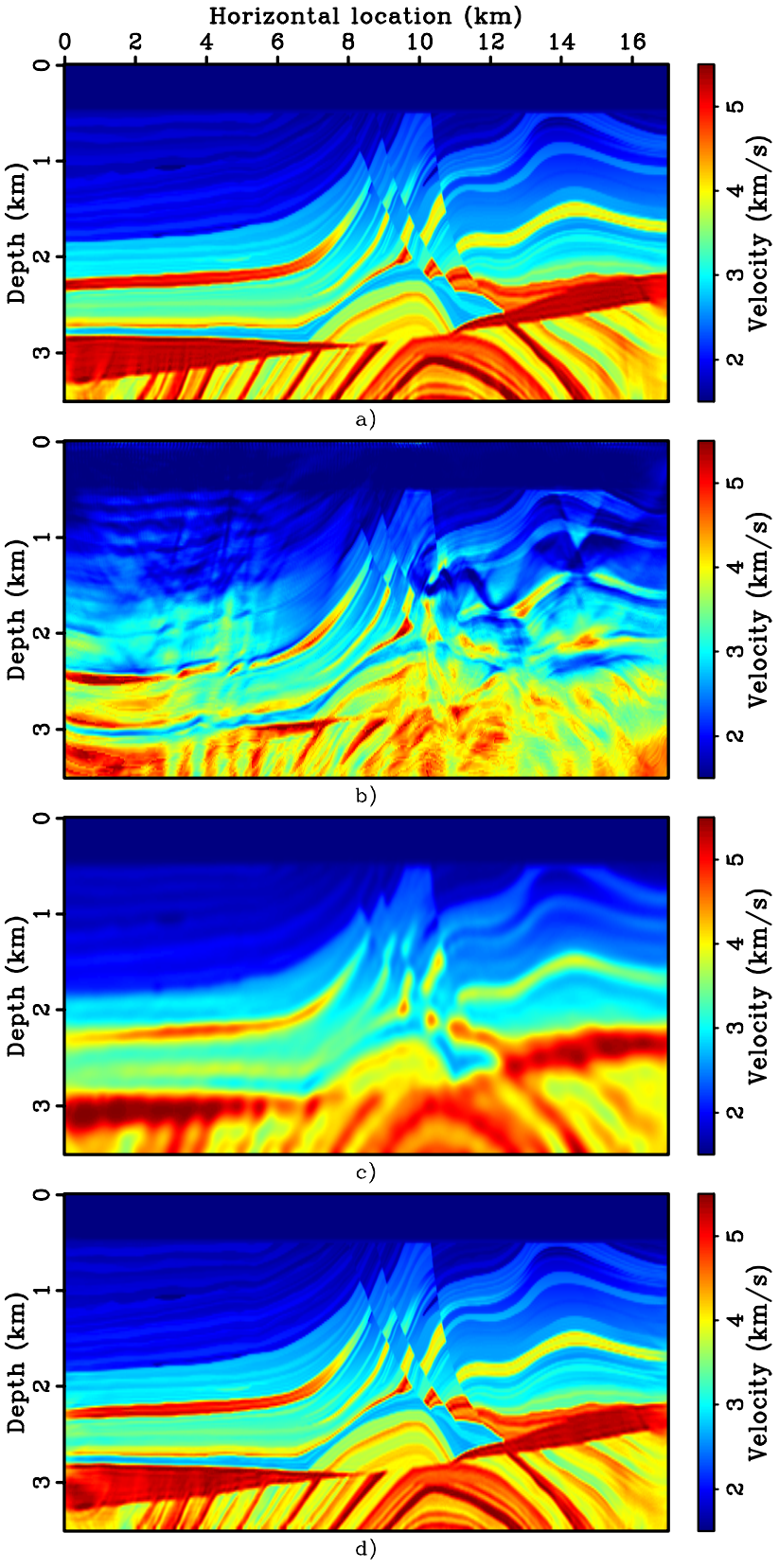

Figure 3: Velocity models estimated from the 3-25 Hz dataset by applying: a) TFWI for the whole bandwidth, b) FWI with frequency continuation starting from 3 Hz data, c) TFWI up to 10 Hz, and d) FWI with frequency continuation starting from 10 Hz data and the model shown in c). [**CR**]

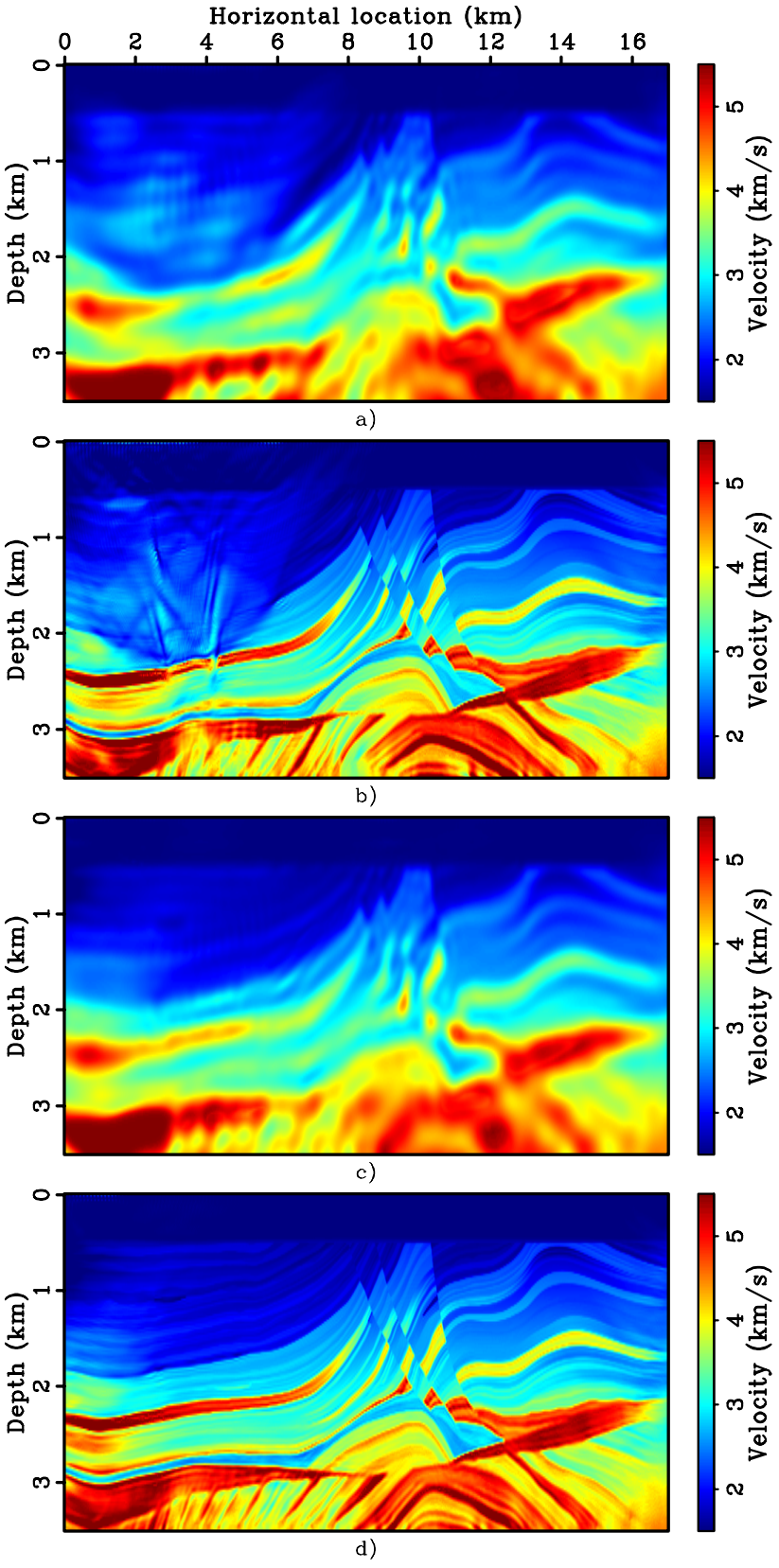

Figure 4: Velocity models estimated from the 5-25 Hz dataset by applying: a) 5 outer iterations of TFWI up to 10 Hz, b) FWI with frequency continuation starting from 10 Hz data and the model shown in a), c) 10 outer iterations of TFWI up to 10 Hz, d) FWI with frequency continuation starting from 10 Hz data and the model shown in c). [**CR**]